nature structural & molecular biology

Energetics and dynamics of SNAREpin folding across lipid bilayers

Feng Li[1], Frédéric Pincet[1], Eric Perez[1], William S Eng[2], Thomas J Melia[2], James E Rothman[2] & David Tareste[2]

Membrane fusion occurs when SNAREpins fold up between lipid bilayers. How much energy is generated during SNAREpin folding and how this energy is coupled to the fusion of apposing membranes is unknown. We have used a surface forces apparatus to determine the energetics and dynamics of SNAREpin formation and characterize the different intermediate structures sampled by cognate SNAREs in the course of their assembly. The interaction energy–versus–distance profiles of assembling SNAREpins reveal that SNARE motifs begin to interact when the membranes are 8 nm apart. Even after very close approach of the bilayers (~2–4 nm), the SNAREpins remain partly unstructured in their membrane-proximal region. The energy stabilizing a single SNAREpin in this configuration (35 k_BT) corresponds closely with the energy needed to fuse outer but not inner leaflets (hemifusion) of pure lipid bilayers (40–50 k_BT).

Intercellular communication and intracellular protein transport rely upon the fusion of cargo-containing vesicles with target membranes. As lipid bilayers are inherently stable, such fusion events are energetically costly and require specialized fusion proteins that harvest the energy made available during their own binding and folding to drive membrane disruption and merging[1–5].

In neuronal synapses, the core of the fusion machinery consists of three proteins from the SNARE family: the synaptic vesicle (v)-SNARE protein VAMP-2 and the two target plasma membrane (t)-SNARE proteins syntaxin-1A and SNAP-25 (refs. 6–8). When separately reconstituted into synthetic liposomes or ectopically expressed on the surfaces of cells, neuronal v- and t-SNARE proteins are sufficient to drive membrane fusion through their assembly in the form of SNAREpins[2,9]. The interacting domains of SNARE proteins (SNARE motifs) contain 60–70 amino acid residues; they are mostly unstructured as monomers[10–12] and assemble in solution into a highly stable heterotrimer consisting of four α-helices aligned in parallel, with VAMP-2 and syntaxin-1A each contributing one helix and SNAP-25 contributing two helices[13,14]. In the context of lipid bilayers, the assembly of SNAREs starts at their membrane-distal N termini and proceeds toward their membrane-proximal C termini (zipper model), a process that also includes passage through a stable intermediate binding state[15–21]. This zipper-like assembly progressively brings the membranes into close apposition and creates a tight bridge between them that triggers lipid bilayer fusion.

Progressive assembly of SNAREs may culminate in a release of energy sufficient to drive membrane merging. Alternatively, the assembling SNAREs may pass through a series of intermediates, each of which contributes enough energy for advancement through the successive stages of membrane fusion. Characterization of these intermediates requires the capacity to measure the interactions between membrane-associated proteins at nanometer distance resolutions.

Thermodynamic and atomic force microscopy (AFM) measurements have successfully described the kinetics of SNARE assembly and disassembly in solution[22] and the rupture forces of SNARE complexes affixed to solid supports[23,24]. However, none of these studies has been able to offer information about the dynamics and energetics of SNAREpin folding, including conformational changes and distance-energy correlations during SNARE assembly. Furthermore, the previous experiments were not performed in the context of lipid bilayers, preventing any investigation of the interplay of lipids and SNARE proteins in membrane interaction and fusion.

Here, we have investigated these questions using the surface forces apparatus (SFA), which directly measures the interaction energy between two facing functionalized membranes as a function of their separation distance and makes it possible to identify molecular rearrangements of interacting species during their association[25]. Direct measurements of force versus distance between membrane-embedded neuronal SNARE proteins (derived from mouse and rat) allow us to explore in real time the molecular details of SNAREpin formation across two lipid bilayers, including conformational changes, kinetics of association, binding energy and extent of assembly.

RESULTS

Interactions between SNAREs in apposing bilayers

Force was measured between two mica-supported lipid bilayers reconstituted with the neuronal cognate t- and v-SNARE proteins (**Fig. 1**). The surfaces were approached toward each other and then

[1]Laboratoire de Physique Statistique, Unité Mixte de Recherche 8550, Centre National de la Recherche Scientifique associée aux Universités Paris VI et Paris VII, Ecole Normale Supérieure, 24 rue Lhomond, 75005 Paris, France. [2]Department of Physiology and Cellular Biophysics, Columbia University, 1150 Saint Nicholas Avenue, New York, New York 10032, USA. Correspondence should be addressed to D.T. (dt2143@columbia.edu).

Received 7 August; accepted 5 September; published online 30 September 2007; doi:10.1038/nsmb1310

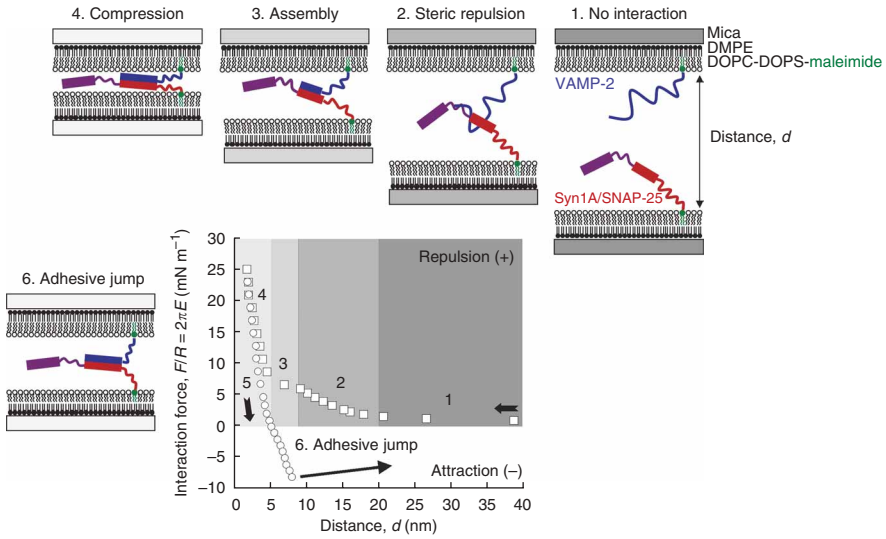

Figure 1 Interaction energy–versus–distance profile of cognate SNAREs in apposing bilayers (squares, approach; circles, separation). Cytoplasmic domains of syntaxin-1A and SNAP-25 (red, with the Habc domain of syntaxin-1A in purple) and VAMP-2 (blue) proteins were chemically anchored to maleimide-containing (green) bilayers via the single cysteine residue introduced at their C-terminal ends. The force, *F*, normalized to the radius of curvature of the surfaces, *R*, is proportional to the corresponding interaction free energy per unit area, *E*, between two equivalent planar surfaces. Upon approach, the interaction between SNARE bilayers proceeds through a series of successive steps depicted in the cartoon. Strong adhesion was measured upon separation (long arrow represents the corresponding adhesive jump). Identical interaction profiles were obtained by repeated cycles of approach and separation, which indicates that SNAREpins can be readily assembled and disassembled in our system. The structures of the SNAREs in the drawing are schematic; they do not necessarily represent the exact configurations of the proteins.

separated from each other with a distance resolution of 1 Å while the corresponding interaction forces were measured with a precision of 1 μN (ref. 26). To study the interactions between SNARE bilayers without the possible complications of subsequent membrane fusion, the transmembrane anchors of SNARE proteins were replaced by a short maleimide lipid that is docking competent but fusion incompetent[27,28]. The cytoplasmic domains of t- and v-SNARE proteins were modified to have only a single cysteine residue at the C-terminal end, and then chemically coupled through this cysteine to a supported lipid bilayer consisting of 89% (mol/mol) neutral phosphatidylcholine lipids (DOPC), 10% (mol/mol) negatively charged phosphatidylserine lipids (DOPS) and 1% (mol/mol) reacting maleimide lipids (DOPE-maleimide). Thus, if every maleimide lipid reacted with a SNARE protein, the average SNARE surface density would be about 1 protein per 70 nm^2; in practice, this density varied across experiments and even across different regions of a bilayer but could be determined accurately for each contact zone tested (see below). We conducted SFA experiments in the protein purification buffer, using many different pairs of cognate SNARE bilayers and probing various regions on these bilayers. The experiments consisted of several approaching/separation cycles during which distances and forces of interaction were measured simultaneously every 30 s.

During the approach of two SNARE bilayers (**Fig. 1**, squares), no force was detected until the membranes reached a separation distance of 20 nm (**Fig. 1**, region 1 of graph), where a long-range exponential repulsive force with a decay length of 8 nm set in (**Fig. 1**, region 2). Given the small Debye screening length of the buffer (0.8 nm), this force cannot have an electrostatic origin but rather corresponds to steric repulsions between exposed SNARE proteins, which begin to overlap at this distance. The long-range exponential repulsion reached a plateau located between 8 nm and 6 nm (**Fig. 1**, region 3) and was followed by a steeper short-range exponential repulsion with a 2- to 3-nm decay length (**Fig. 1**, region 4) that persisted until the two surfaces came into contact. The plateau observed around 8 nm indicates that SNARE proteins do not offer any resistance to compression at this distance. As folded proteins occupy less volume than unfolded proteins and therefore produce weaker steric repulsion, this plateau is the signature of conformational changes occurring within interacting SNARE assemblies and probably corresponds to the region where SNAREpins start to fold up between lipid bilayers. The subsequent short-range repulsions result from further compression of the newly assembled SNAREpins. The minimum bilayer-bilayer distance that could be reached, even under the application of a strong pushing force (25 mN m^{-1} for the data shown here), was about 2 nm. This distance corresponds to the width of a single fully assembled SNARE complex[13,14] and thus probably reflects the thickness of SNAREpins that bridge the two lipid bilayers.

During the separation phase (**Fig. 1**, region 5, data shown as circles), the force-versus-distance profile at first coincided perfectly with that of the approaching phase. However, starting at about 5 nm, the curves diverged, and the transition plateau was no longer evident. Even as the pushing force was reduced down to zero and, eventually, as pulling forces were applied, the surfaces remained in close contact. This hysteresis in the approaching/separation cycle indicates that SNAREpins stay assembled even upon the application of strong pulling forces. During this phase, the separation distance only moderately increases, owing to stretching of the flexible and unassembled parts of the SNARE complexes. When the applied pulling force equals the force that binds the two SNARE bilayers, the surfaces jump out of contact (**Fig. 1**, point 6). On the profile shown in **Figure 1**, this adhesive jump occurred at around 8 nm with a pull-off force, $F_{t/v}/R$ (where *F* is force, t/v denotes the use of a t-SNARE/v-SNARE pair and *R* is radius of curvature), of 8 mN m^{-1}, which is much stronger than that observed between SNARE-free lipid bilayers (**Supplementary Fig. 1** and **Supplementary Data** online). Subsequent approaching/separation cycles had identical force-versus-distance profiles, including reproducible pull-off forces and bilayer separation distances at contact (that is, SNAREpins could be readily assembled and disassembled). However, we observed variations in the measured adhesive forces, which ranged from 3 to 20 mN m^{-1}, across pairs of SNARE bilayers tested and across regions probed on these SNARE bilayers (statistics are provided in **Supplementary Table 1** online). Such variations originate from differences in local SNARE surface densities, as observed occasionally in confocal images of fluorescent SNARE bilayers (**Supplementary Fig. 2** online). We were able to quantify these variations by precisely analyzing the long-range, polymer-like steric repulsion experienced by two SNARE bilayers when they approach each other (see below).

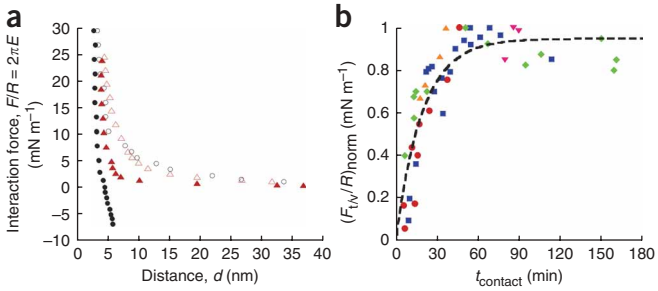

Figure 2 Specificity and kinetics of SNARE assembly. (**a**) Interaction profiles of SNARE bilayers before (circles) and after (triangles) addition of soluble v-SNAREs into the SFA chamber. Open symbols, approach; filled symbols, separation. After 1 h incubation at room temperature, the approaching phase did not show the transition plateau anymore (no conformational changes occurred) and the contact distance was slightly shifted, from about 1 nm, toward larger distances (the protein layer was thicker and/or less compressible). During the separation phase, the force then continuously decreased, eventually reaching the baseline of forces (no adhesion was observed). (**b**) Kinetics of SNARE-bilayer adhesion. The surfaces were approached and kept in contact for a given period of time before being separated. $t_{contact}$ includes the waiting time in contact and the duration of the separation phase. Each symbol corresponds to a different pair of SNARE bilayers, and each data point represents a different approaching/separation cycle. For each pair tested, the adhesion energy was normalized to the maximal adhesion energy measured during the several approaching/separation cycles performed. SNARE bilayers reach their optimal adhesive state within tens of minutes, which we attribute to collective molecular rearrangements.

The specificity of cognate SNARE bilayer interactions was confirmed by the ability of soluble v-SNAREs to inhibit the adhesion of SNARE bilayers (**Fig. 2a**). When soluble v-SNAREs were added between cycles (after SNARE binding was observed), subsequent force-versus-distance profiles showed no structural rearrangements during the approaching phase and no adhesive jump during the separation.

Through their assembly in the form of SNAREpins, cognate t- and v-SNARE proteins are therefore able to produce strong and specific bonds between two lipid membranes in which they are embedded. In addition, the distance of the adhesive jump is consistent with a majority of SNAREpins assembling into a parallel configuration[29] (**Supplementary Fig. 3** online).

Kinetics of SNARE assembly

The repulsion profile of two approaching SNARE bilayers (**Fig. 1**, regions 2–4) offers insight into the kinetics of SNAREpin folding. A plateau is evident, beginning around 8 nm, that corresponds to the transition from long-range repulsive forces (between unbound cognate SNAREs) to short-range repulsive forces (arising from the compression of assembling SNAREpins). This inflection in the repulsion profile occurs during the time between two consecutive measurements—that is, within 30 s. Because the time resolution of the SFA measurements is 30 s, we could not get more than one data point in this region; however, this feature was always observed. The first signs of structural changes, and therefore of SNAREpin formation, thus appear rapidly, within less than 1 min. As we measured forces between macroscopic regions on the bilayer, with up to 10^5 SNAREpins in the contact zone, this represents the association kinetics of a population of SNARE complexes.

This assembly phase probably corresponds to the transition from docking to priming *in vivo*[30], whereas the docking step—the approach of membranes as close as tens of nanometers apart, normally mediated by Rab GTPases and their effectors—is mimicked here by the mechanical approach of two SNARE bilayers. In chromaffin cells, which use the same fusion machinery that functions in neurons, it takes tens of seconds for the large dense-core vesicles to transit from a pool of docked but unprimed vesicles to a pool of fusion-ready vesicles[31]. Slightly faster rate constants (within seconds) have been measured for the formation of the readily releasable pool of synaptic vesicles[32]. However, SNARE assembly is very probably assisted by other factors *in vivo* (for example, Munc13 (ref. 31) or Munc18 (ref. 33)). The speed at which SNAREpin folding is initiated between our reconstituted SNARE bilayers is therefore consistent with physiological studies.

Next, we investigated the kinetics of development of an optimal adhesive state. To this end, we measured forces while SNARE bilayers were approached and kept in contact for various periods of time before being separated. The relevant parameter is therefore the contact time between the two surfaces, $t_{contact}$, which is defined as the time that elapses between the end of the approaching phase and the adhesive jump. The adhesion at each contact zone tested could then be normalized to the maximal adhesion measured in the course of the several approaching/separation cycles we performed. The resulting plot of $(F_{t/v}/R)_{norm}$ against $t_{contact}$ increases exponentially, reaching half its maximal value in 15 min and plateauing after about 60 min (**Fig. 2b**).

The bridging of two lipid bilayers by isolated SNAREpins is therefore composed of two kinetic components: a fast component (tens of seconds) that corresponds to the initiation of SNAREpin folding and a slow component (tens of minutes) leading to an optimized adhesive force that may be inherent to our system and probably originates from collective molecular rearrangements.

SNAREpin binding energy

Membrane fusion proceeds through a series of intermediate stages that include membrane approach and deformation (with the potential creation of a hemifusion structure), pore formation and pore enlargement. Each of these stages is highly energy consuming, requiring about 40–50 k_BT (ref. 5). What, then, is the energy released upon SNAREpin formation?

The binding energy per SNAREpin, $e_{t/v}$, can be deduced from the macroscopic adhesion energy of two SNARE bilayers, $E_{t/v}$, and the surface density of SNARE proteins, Γ_S, via the equation

$$E_{t/v} = \Gamma_S e_{t/v} \quad (1)$$

where $E_{t/v}$ is related to the measured pull-off force, $F_{t/v}/R$, by the equation[34,35]

$$E_{t/v} = F_{t/v}/2\pi R \quad (2)$$

To describe accurately the binding energy per SNAREpin, we therefore had to determine the surface density of SNARE proteins and use the maximal adhesion energy—that is, the adhesion energy when all of the SNAREpins are engaged.

Notably, we observed a correlation between stronger adhesive forces and larger long-range steric repulsive forces (**Supplementary Fig. 4** online). This suggests that variations in the measured adhesive forces are due to variations in SNARE surface density and that the latter can

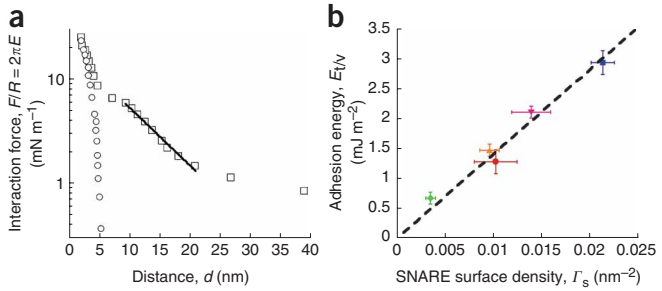

Figure 3 Energy of SNAREpin folding. (**a**) Measurement of SNARE surface density. During the approaching phase and before they form structured complexes (between 20 nm and 9 nm), cognate SNAREs can be treated as random polymers in a mushroom configuration. The transition from unbound to bound states appears as an inflection in the interaction profile (located at about 8 nm). The long-range steric repulsion between SNARE bilayers (plotted on a logarithmic scale) is fit well by the energy equation of the mushroom model (solid line), which allows us to deduce the surface density of SNAREs, Γ_S. (**b**) SNAREpin binding energy. The adhesion energy of SNARE bilayers, $E_{t/v}$, is plotted as a function of Γ_S deduced from the polymer model. Each symbol corresponds to a different pair of SNARE bilayers; adhesion values plotted are means and error bars show s.e.m. from $n = 3$–18 approaching/separation cycles (see **Supplementary Table 1** for details). The plot can be fit by a straight line whose slope gives the binding energy per SNAREpin, $e_{t/v} = 35 \pm 7\ k_BT$.

be deduced from a careful analysis of the repulsive parts of the interaction profiles. To model long-range steric repulsions experienced by SNARE bilayers during the approaching phase, we tested two well-described theories regarding steric forces between polymer surfaces (**Supplementary Data**): the 'mushroom' and 'brush' theories developed for surfaces of low and high polymer densities, respectively[36–39]. Our force measurements are fit well by an energy equation based on the mushroom theory (**Fig. 3a**), whereas the brush theory led to illogical results: the thickness of the brush would decrease as the density increased (**Supplementary Fig. 5** online). SNARE surface densities deduced from mushroom-theory fits ranged from 1 protein per 47 nm^2 to 1 protein per 284 nm^2, with an average of 1 protein per 121 nm^2, which is very close to the density of VAMP-2 found on synaptic vesicles[40]. It may be surprising that simple polymer scaling theories can model so well the steric repulsions between SNARE protein surfaces. This is, however, consistent with structural properties of individual SNAREs and scaling models recently developed for globular proteins. The cytoplasmic domain of the v-SNARE is largely unstructured in solution[10,12] and can therefore be represented as a random coil[41,42]. The cytoplasmic domain of the t-SNARE complex consists of several α-helical segments interconnected by unstructured linkers[43–46], and its dimensions can also be predicted reasonably well by random-coil statistics[47].

Knowing both the optimal adhesion energy for each given pair of SNARE bilayers and the surface density of SNAREs, we were able to plot $E_{t/v}$ versus Γ_S. The resulting curve can be fit by a straight line whose slope gives the binding energy per SNAREpin, $e_{t/v} = 35 \pm 7\ k_BT$ (**Fig. 3b**). This linear relationship between $E_{t/v}$ and Γ_S validates *a posteriori* the use of the mushroom theory to describe long-range steric repulsions between SNARE bilayers and confirms that variations in the measured adhesive forces originate from variations in SNARE surface density.

The $e_{t/v}$ measured here represents the energy difference between the bound and unbound states. As such, it corresponds (i) to the overall energy required to dissociate the SNAREpin and also (ii) to the energy liberated by each SNAREpin formation (energy available for fusion).

We also estimated the rate of spontaneous SNAREpin dissociation, given by[48]

$$t = t_0 \exp\left(\frac{e_{t/v,a}}{k_B T}\right) \quad (3)$$

where t_0, the diffusive relaxation time of the bond, is on the order of 10^{-9} s in condensed liquids or inside compact structures such as proteins[49], and where $e_{t/v,a}$ is the activation energy of the bond (the energy barrier that the bond must overcome to dissociate, which is usually larger than the binding energy). By inserting the $e_{t/v}$ calculated above into equation (3), we obtained a lower bound of the lifetime of the bond, which establishes that the SNAREpin has a lifetime of at least several days—in other words, that it is irreversible on biological timescales.

Extent of SNAREpin assembly

The binding energy of 35 k_BT described above refers to the culmination of a stable assembly state in SNAREpin development. Because of the tight control over distance afforded by the SFA, we were also able to ascertain at which distance this energy develops, whether it is progressively increasing during the approach or marks a jump to a stable intermediate, and whether or not this represents an intermediate or final assembly state.

To do this, we studied successive approaching/separation cycles during which the minimal approaching distance (contact distance) between SNARE bilayers, d_{min}, was progressively decreased. To account for the slow kinetics of population assembly, we considered only interaction profiles with contact times longer than 30 min (this gives the SNARE bilayers enough time to reach an optimal adhesive state). The adhesion energies were normalized to the surface density of SNAREs, Γ_S, and plotted as the mean adhesion energy per SNARE complex, e_m. When the two surfaces were never closer than 9 nm before being separated, almost no adhesion was detected. A sharp transition to a high-adhesion regime occurred when the surfaces were

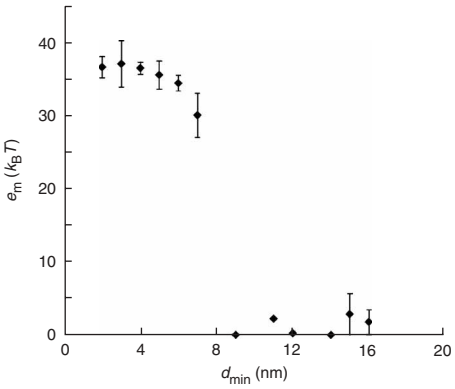

Figure 4 Extent of SNAREpin folding. A series of approaching/separation cycles was performed in which the contact distance, d_{min}, was varied. SNARE bilayers were allowed to interact long enough to reach their optimal adhesive state ($t_{contact} \geq 30$ min) before being separated. Adhesion energies were normalized to SNARE surface densities. Data were gathered for each 1 nm and, for each ensemble, the mean adhesion and s.e.m. were calculated ($n = 2$–12 adhesion values). The transition from no adhesion to high adhesion is very steep and occurs at about 8 nm. The adhesion increases slightly between 7 and 4 nm, and does not vary between 4 and 2 nm, suggesting that, in our system, SNARE zippering comes to a stop once the bilayers are 4 nm apart.

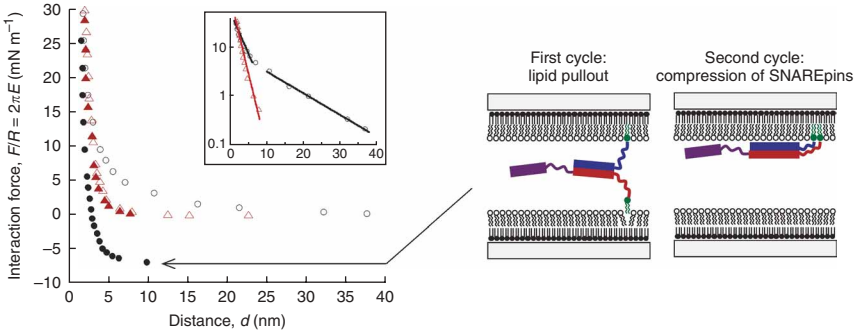

Figure 5 SNARE assembly and adhesion energy are modulated by SNARE-membrane interactions. Forces were measured in the absence of negatively charged DOPS lipids in the bilayers (we tested two independent pairs of SNARE bilayers, probing various regions on these bilayers). Open symbols, approach; filled symbols, separation. Inset shows the approaching phases on a semi-log scale to highlight the different exponential repulsion regimes (fit by solid lines). The force-versus-distance profile is not reversible in this case (cycle 1, circles; cycle 2, triangles): the second approaching/separation cycle shows a single repulsion regime during the approach (corresponding to the compression of the previously assembled SNAREpins) and no adhesion during the separation. This indicates that lipid-anchored SNAREs are pulled out of the bilayers during the first cycle, a result of either weaker anchorage or a more stable SNAREpin, or both (see text). Configurations of the proteins in the cartoons are hypothetical.

brought down to 8 nm (**Fig. 4**). For $d_{min} \leq 7$ nm, the adhesion increased slowly and reached a plateau around 4 nm. The surfaces could then be approached as close as 2 nm from each other without any noticeable increase of their adhesion.

Therefore, SNARE motifs start to assemble and to form substantially stable SNAREpins when the distance between lipid bilayers is 8 nm. The minimal distance between SNARE bilayers that we were able to reach (2 nm) is in good agreement with the known crystal structure of the SNARE complex[13,14] and suggests a configuration where SNARE motifs are aligned parallel to the plane of the membranes. The absence of any further increase of adhesion in the region $2 \text{ nm} \leq d_{min} \leq 4$ nm suggests that by 4 nm we reached a stop in the formation of energetically favorable coiled coils. In other words, SNAREpins can assemble only partially when cognate SNAREs are isolated in supported lipid bilayers.

SNAREpins are, by definition, a transient intermediate on the pathway to fusion, and such partially assembled coiled coils have already been observed in both *in vivo* and *in vitro* systems[16–19,21]. Typically, the degree of assembly is inferred by probing the sensitivity of SNAREpins to antibodies or neurotoxins that bind specific regions of the SNARE sequence. Unfortunately, the large contact area between our supported SNARE bilayers renders the SNARE motifs inaccessible to such soluble factors. Instead, we estimated the number of unstructured residues from the distance the two bilayers could be separated before the adhesive jump, during the phase when the unassembled C-terminal parts of the SNAREs are stretched (**Supplementary Data**). The average jump-out distance of 9 nm (**Supplementary Table 1**) implies that 12–25 membrane-proximal amino acid residues of each SNARE are unstructured and have not entered into a stable SNARE bundle. Thus, 35 k_BT represents the energy captured in an incompletely assembled SNAREpin.

SNARE assembly modulated by SNARE-membrane interactions

Within the membrane-proximal region of the unstructured SNARE sequence are positively charged residues that can interact electrostatically with negative lipids in the membrane[50–52]. To address whether this electrostatic interaction has a role in SNAREpin assembly and adhesion energy, we measured forces in the absence of negatively charged DOPS lipids in the bilayers. In this case, the interaction profile of the SNARE bilayers was not reversible: after a first cycle of approach and separation with strong adhesion, subsequent cycles resulted in no conformational change during the approach and no adhesion during the separation (**Fig. 5**). This indicates that the maleimide lipids to which the SNAREs are anchored are pulled out of the outer monolayers during the separation process. In this configuration, the energy needed to separate the SNAREs is therefore larger than that required to extract a lipid from a bilayer structure (30–40 k_BT (ref. 53); see also **Supplementary Data**), an observation which could arise from either weaker SNARE anchorage or a more energetic (further assembled) SNAREpin, or both. Either case implies some electrostatic interaction between the membrane-proximal residues of SNAREs and the DOPS lipids (interaction that stabilizes SNARE anchorage in the first case and sequesters SNARE motifs in the second). Such an interaction between SNAREs and the membrane could contribute to the prevention of full SNAREpin assembly we have observed here. *In vivo*, this interaction could act as a regulator of SNARE assembly in conjunction with electrostatic switches; the switches could include, for example, the synaptotagmins, through their calcium-dependent mode of binding to SNAREpins and/or phospholipids[8,54]. Electrostatic interactions could also be used to transmit the energy released during SNAREpin folding to the transmembrane domains of cognate SNAREs and the surrounding lipids[52].

DISCUSSION

To date, SFA measurements have been limited to static molecular assemblies whose interactions were either structural (for example, DNA base-pairing[55,56]) or responsible for initiating a signaling cascade (for example, streptavidin-biotin[57] or cadherin-cadherin interactions[58]). Molecules like the SNAREs that use a highly dynamic association process to do actual work on the lipid bilayers have not previously been explored. Here, we have identified the successive stages of SNARE assembly, including the initiation of binding and subsequent conformational changes, and precisely quantified the molecular adhesion energy (**Supplementary Fig. 6** online). Our study shows that SNAREpin folding is initiated when cognate SNARE membranes are 8 nm apart. In the cell, docking factors, such as Rabs and tethers, would facilitate this transition by reducing the cytosolic gap to this distance. As the membranes are progressively pulled together, an increasing amount of energy is stored in the folding SNAREpin, and this energy reaches a plateau when the intermembrane distance is ~4 nm. The resulting SNAREpin is partially unstructured in its C-terminal region and provides a highly stable membrane-bridging complex, irreversible on biological timescales, that is probably the physiologically relevant substrate for many regulatory factors (for example, complexin[59] or synaptotagmin[8,54]). In our system, membrane-proximal regions of SNAREs interact with the membrane structure itself; this could have a role in functionally coupling SNARE assembly to the bending and fusion of two apposing bilayers. Notably, our SFA data show that the energy accumulated

during such partial SNAREpin folding across two membranes is 35 k_BT, which is already very close to the energy required to create the highly curved non-bilayer transition structures (stalks) that lead to fusion (40–50 k_BT)[60].

METHODS

Protein expression and purification. The soluble t-SNARE complex—made up of the cytoplasmic domain of rat syntaxin-1A containing a single C-terminal cysteine residue (encoded on pJM57) and mouse His_6–SNAP-25 with no cysteine residues (pJM72)—and the cytoplasmic domain of mouse His_6–VAMP-2 containing a C-terminal cysteine residue (pJM51) were expressed and purified essentially as described[28] (see **Supplementary Methods** online for minor modifications).

SNARE bilayer reconstitution. SNARE bilayers were formed on silvered mica surfaces using Langmuir-Blodgett deposition[61]. A first monolayer of 1,2-dimyristoyl-*sn*-glycero-3-phosphoethanolamine (DMPE) lipids was deposited in a solid state, at 38 mN m^{-1}, with its headgroups facing the mica surface. A second monolayer made up of a mixture of 89% (mol/mol) 1,2-dioleoyl-*sn*-glycero-3-phosphocholine (DOPC), 10% (mol/mol) 1,2-dioleoyl-*sn*-glycero-3-(phospho-L-serine) (DOPS), and 1% (mol/mol) 1,2-dioleoyl-*sn*-glycero-3-phosphoethanolamine-*N*-(4-(*p*-maleimidophenyl)butyramide) (DOPE-maleimide) was deposited in a fluid state, at 35 mN m^{-1}, with its headgroups facing the aqueous buffer. These Langmuir-Blodgett depositions were performed in pure water. Next, the lipidic bilayers were transferred into the coupling buffer (25 mM HEPES-KOH (pH 7.6), 100 mM KCl, 0.25 mM Tris(2-carboxyethyl)phosphine (TCEP)), where SNARE proteins were anchored to the DOPE-maleimide headgroups via the single cysteine residue introduced at the C terminus of each protein (see **Supplementary Methods** for detailed protocol).

Surface force measurements. Force measurements were carried out with a homemade SFA similar to Israelachvili's design[26]. The SFA measures the force, F, between two crossed-cylindrical mica surfaces as a function of their separation distance, d. F is obtained from the deflection of a leaf spring that supports one of the two micas with a precision of 1 μN. d is measured by multiple-beam interferometry with a resolution of 1 Å.

The crossed-cylinder geometry of the SFA is equivalent to a sphere-plane geometry, which means that many bonds are simultaneously formed at various distances. The force measured at a given distance is therefore the sum of all the forces at distances varying from the closest distance to infinity. At equilibrium, this sum is proportional to the interaction free energy per unit area, E, between two equivalent planar surfaces at a distance d (the energy being zero when the surfaces are at an infinite distance from each other).

The ratio F/R, where $R = 2$ cm is the mean radius of curvature of the two mica surfaces, is related by the Derjaguin approximation[34] to the corresponding interaction free energy per unit area, E, between two equivalent planar surfaces:

$$F/R = 2\pi E \qquad (4)$$

The net force obtained from SFA measurements is the total force integrated over the whole contact area between the two surfaces (about 10 μm^2). In the context of SNARE-bilayer force measurements, it therefore gives the interaction free energy of all proteins within the contact area (about 10^5 proteins).

All SNARE-bilayer force measurements were carried out at 21 °C in degassed coupling buffer (25 mM HEPES-KOH (pH 7.6), 100 mM KCl, 0.25 mM TCEP), using a spring stiffness of 130 N m^{-1}.

Definition of the intersurface separation distance. In all force-versus-distance profiles presented in this paper, the reference distance $d = 0$ corresponds to the hydrophilic contact between two DMPE//DOPC–DOPS–DOPE-maleimide bilayers (where // separates the compositions of the inner and outer monolayers; see **Fig. 1**).

In the course of SFA experiments, it is more convenient to use the reference distance $D = 0$, where D refers to the separation distance between the hydrophobic DMPE surfaces. This distance was determined at the end of each experiment by draining the aqueous buffer slowly from the apparatus, which removes the outer lipid monolayers and therefore exposes only the inner hydrophobic DMPE monolayers, and then bringing these two monolayers into contact in air.

Therefore, we first measured forces between protein-free bilayers to obtain the thickness, T, of two contacting DOPC–DOPS–DOPE-maleimide monolayers; we found $T = 6$ nm. This thickness was then subtracted from D, determined in the course of SNARE-bilayer force measurements, to give the interbilayer separation distance $d = D - 6$ nm.

Note: Supplementary information is available on the Nature Structural & Molecular Biology website.

ACKNOWLEDGMENTS

This work was supported by the Human Frontier Science Program, a travel grant from US National Science Foundation, and US National Institutes of Health grants to J.E.R. We thank J. McNew (Rice University) for the generous gift of the plasmids used in this study, and A. Martin-Molina, A. Yamamoto and D. You for experimental help and many fruitful discussions.

Published online at http://www.nature.com/nsmb
Reprints and permissions information is available online at http://npg.nature.com/reprintsandpermissions

1. Sollner, T., Bennett, M.K., Whiteheart, S.W., Scheller, R.H. & Rothman, J.E. A protein assembly-disassembly pathway in-vitro that may correspond to sequential steps of synaptic vesicle docking, activation, and fusion. *Cell* **75**, 409–418 (1993).
2. Weber, T. *et al.* SNAREpins: minimal machinery for membrane fusion. *Cell* **92**, 759–772 (1998).
3. Chernomordik, L.V. & Kozlov, M.M. Protein-lipid interplay in fusion and fission of biological membranes. *Annu. Rev. Biochem.* **72**, 175–207 (2003).
4. Tamm, L.K., Crane, J. & Kiessling, V. Membrane fusion: a structural perspective on the interplay of lipids and proteins. *Curr. Opin. Struct. Biol.* **13**, 453–466 (2003).
5. Cohen, F.S. & Melikyan, G.B. The energetics of membrane fusion from binding, through hemifusion, pore formation, and pore enlargement. *J. Membr. Biol.* **199**, 1–14 (2004).
6. Sollner, T. *et al.* SNAP receptors implicated in vesicle targeting and fusion. *Nature* **362**, 318–324 (1993).
7. Brunger, A.T. Structure and function of SNARE and SNARE-interacting proteins. *Q. Rev. Biophys.* **38**, 1–47 (2005).
8. Jackson, M.B. & Chapman, E.R. Fusion pores and fusion machines in Ca2+-triggered exocytosis. *Annu. Rev. Biophys. Biomol. Struct.* **35**, 135–160 (2006).
9. Hu, C. *et al.* Fusion of cells by flipped SNAREs. *Science* **300**, 1745–1749 (2003).
10. Fasshauer, D., Otto, H., Eliason, W.K., Jahn, R. & Brunger, A.T. Structural changes are associated with soluble N-ethylmaleimide-sensitive fusion protein attachment protein receptor complex formation. *J. Biol. Chem.* **272**, 28036–28041 (1997).
11. Dulubova, I. *et al.* A conformational switch in syntaxin during exocytosis: role of munc18. *EMBO J.* **18**, 4372–4382 (1999).
12. Hazzard, J., Sudhof, T.C. & Rizo, J. NMR analysis of the structure of synaptobrevin and of its interaction with syntaxin. *J. Biomol. NMR* **14**, 203–207 (1999).
13. Poirier, M.A. *et al.* The synaptic SNARE complex is a parallel four-stranded helical bundle. *Nat. Struct. Biol.* **5**, 765–769 (1998).
14. Sutton, R.B., Fasshauer, D., Jahn, R. & Brunger, A.T. Crystal structure of a SNARE complex involved in synaptic exocytosis at 2.4 Å resolution. *Nature* **395**, 347–353 (1998).
15. Hanson, P.I., Roth, R., Morisaki, H., Jahn, R. & Heuser, J.E. Structure and conformational changes in NSF and its membrane receptor complexes visualized by quick-freeze/deep-etch electron microscopy. *Cell* **90**, 523–535 (1997).
16. Hua, S.Y. & Charlton, M.P. Activity-dependent changes in partial VAMP complexes during neurotransmitter release. *Nat. Neurosci.* **2**, 1078–1083 (1999).
17. Xu, T. *et al.* Inhibition of SNARE complex assembly differentially affects kinetic components of exocytosis. *Cell* **99**, 713–722 (1999).
18. Chen, Y.A., Scales, S.J. & Scheller, R.H. Sequential SNARE assembly underlies priming and triggering of exocytosis. *Neuron* **30**, 161–170 (2001).
19. Melia, T.J. *et al.* Regulation of membrane fusion by the membrane-proximal coil of the t-SNARE during zippering of SNAREpins. *J. Cell Biol.* **158**, 929–940 (2002).
20. Sorensen, J.B. *et al.* Sequential N- to C-terminal SNARE complex assembly drives priming and fusion of secretory vesicles. *EMBO J.* **25**, 955–966 (2006).
21. Pobbati, A.V., Stein, A. & Fasshauer, D. N- to C-terminal SNARE complex assembly promotes rapid membrane fusion. *Science* **313**, 673–676 (2006).
22. Fasshauer, D., Antonin, W., Subramaniam, V. & Jahn, R. SNARE assembly and disassembly exhibit a pronounced hysteresis. *Nat. Struct. Biol.* **9**, 144–151 (2002).
23. Liu, W. *et al.* Single molecule mechanical probing of the SNARE protein interactions. *Biophys. J.* **91**, 744–758 (2006).
24. Yersin, A. *et al.* Interactions between synaptic vesicle fusion proteins explored by atomic force microscopy. *Proc. Natl. Acad. Sci. USA* **100**, 8736–8741 (2003).
25. Israelachvili, J.N. *Intermolecular and Surface Forces* (Academic Press, London, 1992).
26. Israelachvili, J.N. & Adams, G.E. Measurement of forces between 2 mica surfaces in aqueous-electrolyte solutions in range 0–100 nm. *J. Chem. Soc. Farad. Trans. I* **74**, 975–1001 (1978).
27. Grote, E., Baba, M., Ohsumi, Y. & Novick, P.J. Geranylgeranylated SNAREs are dominant inhibitors of membrane fusion. *J. Cell Biol.* **151**, 453–465 (2000).

28. McNew, J.A. *et al.* Close is not enough: SNARE-dependent membrane fusion requires an active mechanism that transduces force to membrane anchors. *J. Cell Biol.* **150**, 105–117 (2000).
29. Bowen, M.E., Weninger, K., Brunger, A.T. & Chu, S. Single molecule observation of liposome-bilayer fusion thermally induced by soluble N-ethyl maleimide sensitive-factor attachment protein receptors (SNAREs). *Biophys. J.* **87**, 3569–3584 (2004).
30. Rettig, J. & Neher, E. Emerging roles of presynaptic proteins in Ca++-triggered exocytosis. *Science* **298**, 781–785 (2002).
31. Ashery, U. *et al.* Munc13–1 acts as a priming factor for large dense-core vesicles in bovine chromaffin cells. *EMBO J.* **19**, 3586–3596 (2000).
32. Rizzoli, S.O. & Betz, W.J. Synaptic vesicle pools. *Nat. Rev. Neurosci.* **6**, 57–69 (2005).
33. Shen, J., Tareste, D.C., Paumet, F., Rothman, J.E. & Melia, T.J. Selective activation of cognate SNAREpins by Sec1/Munc18 proteins. *Cell* **128**, 183–195 (2007).
34. Derjaguin, B.V., Muller, V.M. & Toporov, Y.P. Effect of Contact Deformations on Adhesion of Particles. *J. Colloid Interface Sci.* **53**, 314–326 (1975).
35. Maugis, D. Adhesion of spheres—the Jkr-Dmt transition using a dugdale model. *J. Colloid Interface Sci.* **150**, 243–269 (1992).
36. Dolan, A.K. & Edwards, S.F. Theory of stabilization of colloids by adsorbed polymer. *Proc. R. Soc. Lond. B Math. Phys. Eng. Sci.* **337**, 509–516 (1974).
37. Alexander, S. Adsorption of chain molecules with a polar head a-scaling description. *J. Physique* **38**, 983–987 (1977).
38. Degennes, P.G. Polymers at an interface—a simplified view. *Adv. Colloid Interface Sci.* **27**, 189–209 (1987).
39. Kuhl, T.L., Leckband, D.E., Lasic, D.D. & Israelachvili, J.N. Modulation of interaction forces between bilayers exposing short-chained ethylene-oxide headgroups. *Biophys. J.* **66**, 1479–1488 (1994).
40. Takamori, S. *et al.* Molecular anatomy of a trafficking organelle. *Cell* **127**, 831–846 (2006).
41. Millett, I.S., Doniach, S. & Plaxco, K.W. Toward a taxonomy of the denatured state: small angle scattering studies of unfolded proteins. *Adv. Protein Chem.* **62**, 241–262 (2002).
42. Kohn, J.E. *et al.* Random-coil behavior and the dimensions of chemically unfolded proteins. *Proc. Natl. Acad. Sci. USA* **101**, 12491–12496 (2004).
43. Fernandez, I. *et al.* Three-dimensional structure of an evolutionarily conserved N-terminal domain of syntaxin 1A. *Cell* **94**, 841–849 (1998).
44. Margittai, M., Fasshauer, D., Pabst, S., Jahn, R. & Langen, R. Homo- and hetero-oligomeric SNARE complexes studied by site-directed spin labeling. *J. Biol. Chem.* **276**, 13169–13177 (2001).
45. Xiao, W., Poirier, M.A., Bennett, M.K. & Shin, Y.K. The neuronal t-SNARE complex is a parallel four-helix bundle. *Nat. Struct. Biol.* **8**, 308–311 (2001).
46. Margittai, M., Fasshauer, D., Jahn, R. & Langen, R. The Habc domain and the SNARE core complex are connected by a highly flexible linker. *Biochemistry* **42**, 4009–4014 (2003).
47. Fitzkee, N.C. & Rose, G.D. Reassessing random-coil statistics in unfolded proteins. *Proc. Natl. Acad. Sci. USA* **101**, 12497–12502 (2004).
48. Hanggi, P., Talkner, P. & Borkovec, M. Reaction-rate theory—50 years after Kramers. *Rev. Mod. Phys.* **62**, 251–341 (1990).
49. Evans, E. Probing the relation between force–lifetime–and chemistry in single molecular bonds. *Annu. Rev. Biophys. Biomol. Struct.* **30**, 105–128 (2001).
50. Hu, K. *et al.* Vesicular restriction of synaptobrevin suggests a role for calcium in membrane fusion. *Nature* **415**, 646–650 (2002).
51. Kim, C.S., Kweon, D.H. & Shin, Y.K. Membrane topologies of neuronal SNARE folding intermediates. *Biochemistry* **41**, 10928–10933 (2002).
52. Knecht, V. & Grubmuller, H. Mechanical coupling via the membrane fusion SNARE protein syntaxin 1A: a molecular dynamics study. *Biophys. J.* **84**, 1527–1547 (2003).
53. Marrink, S.J., Berger, O., Tieleman, P. & Jahnig, F. Adhesion forces of lipids in a phospholipid membrane studied by molecular dynamics simulations. *Biophys. J.* **74**, 931–943 (1998).
54. Rizo, J., Chen, X. & Arac, D. Unraveling the mechanisms of synaptotagmin and SNARE function in neurotransmitter release. *Trends Cell Biol.* **16**, 339–350 (2006).
55. Pincet, F., Perez, E., Bryant, G., Lebeau, L. & Mioskowski, C. Long-range attraction between nucleosides with short-range specificity: Direct measurements. *Phys. Rev. Lett.* **73**, 2780–2783 (1994).
56. Tareste, D. *et al.* Energy of hydrogen bonds probed by the adhesion of functionalized lipid layers. *Biophys. J.* **83**, 3675–3681 (2002).
57. Helm, C.A., Knoll, W. & Israelachvili, J.N. Measurement of ligand-receptor interactions. *Proc. Natl. Acad. Sci. USA* **88**, 8169–8173 (1991).
58. Sivasankar, S., Brieher, W., Lavrik, N., Gumbiner, B. & Leckband, D. Direct molecular force measurements of multiple adhesive interactions between cadherin ectodomains. *Proc. Natl. Acad. Sci. USA* **96**, 11820–11824 (1999).
59. Giraudo, C.G., Eng, W.S., Melia, T.J. & Rothman, J.E. A clamping mechanism involved in SNARE-dependent exocytosis. *Science* **313**, 676–680 (2006).
60. Kozlovsky, Y. & Kozlov, M.M. Stalk model of membrane fusion: solution of energy crisis. *Biophys. J.* **82**, 882–895 (2002).
61. Marra, J. Controlled deposition of lipid monolayers and bilayers onto mica and direct force measurements between galactolipid bilayers in aqueous-solutions. *J. Colloid Interface Sci.* **107**, 446–458 (1985).